
Representation Disentanglement via Causal Regularization by Identification

Juan Castorena
 CCS-3 Information Sciences
 Los Alamos National Laboratory
 Los Alamos, NM, 87545
 jcastorena@lanl.gov

Abstract

This work focuses on the problem of learning disentangled representations from observational data. Given observations $\{\mathbf{x}^{(i)}\}_{i=1}^N$ drawn from $p(\mathbf{x}|\mathbf{y})$ with generative variables \mathbf{y} admitting the distribution factorization $p(\mathbf{y}) = \prod_c p(\mathbf{y}_c)$, we ask whether learning disentangled representations matching the space of observations with identification guarantees on the posterior $p(\mathbf{z}|\mathbf{x}, \hat{\mathbf{y}}_c)$ for each c , is plausible. We argue modern deep representation learning models of data matching the distributed factorization property are ill-posed with collider bias behaviour; a source of bias producing entanglement between generating variables. Under the rubric of causality, we show this issue can be explained and reconciled under the condition of identifiability; attainable under supervision or a weak-form of it. For this, we propose regularization by identification (ReI), a modular regularization engine designed to align the behavior of large scale DL models with domain knowledge. Empirical evidence shows that enforcing ReI in a variational framework results in interpretable disentangled representations equipped with generalization capabilities to out-of-distribution examples and that aligns nicely with the true expected effect from domain knowledge between generating variables and measurement apparatus.

1 Introduction

One of the principal objectives of learning representations has been that of detecting/recognizing patterns or signatures of measurements to represent the qualitative and quantitative characteristics of the underlying physical processes being sensed. Most of the times sensing as dictated for example by the Nyquist rate [1] acquires sufficient information for detection but leaves potentially unnecessary and redundant information on its measurements. Ideas to reduce such redundancies by representing information as concepts, patterns or features to achieve an economy of information have been the focus of study since its early days [2]. Classical examples include principal component analysis [3] which assumes linear mapping functions along with orthogonality in its parametrizations. Independent component analysis [4] on the other hand, restricts the elements of the parametrizations to be independent using mutual information. However, both of these methods assume all measurements \mathbf{x} live in a low dimensional space, an assumption not applicable in all task contexts.

The standard variational formulation of representation learning frameworks consists in learning from the observables $\mathbf{x} \in \mathbb{R}^N$ a generative model $p_\theta(\mathbf{x}, \mathbf{z}) = p_\theta(\mathbf{x}|\mathbf{z})p_\theta(\mathbf{z})$ whose learned marginal likelihood $p_\theta(\mathbf{x})$ approximates the true $p_{\theta^*}(\mathbf{x})$. The latent variables $\mathbf{z} \in \mathbb{R}^N$ distributed as $p(\mathbf{z})$ are assumed unknown and focus on this problem has concentrated on finding priors parametrized by ϕ that make the marginal and posterior $p_\phi(\mathbf{z}|\mathbf{x})$ tractable. Variational auto-encoders (VAE)'s [5] for example, builds an efficient optimization approach that maximizes the conditional likelihood

$p_\theta(\mathbf{x}|\mathbf{z})$ subject to similarity constraints quantified by the Kullback-Leibler (KL) divergence between a posterior approximate $q_\phi(\mathbf{z}|\mathbf{x})$ and a family of induced latent distribution priors $p(\mathbf{z})$ (typically an isotropic Gaussian). Problem with these group of methods for disentanglement is their focus on learning approximations of the true marginal data distributions without any restriction or guarantees on the prior in modeling the true generative mechanisms [6]. This not only disconnects meaning of the learned latent representations from supporting access to clear explanations and understanding [7] of the true generative processes, but also invokes problems of trust in their lack of robustness to out-of-distribution (OOD) examples [8] while keeping the necessary adjustments for diagnosis and repair [9] obscure [10].

Recent trends [11, 12, 13, 14, 6] are in consensus that disentanglement of the generating factors leads to increased robust representations that are less susceptible to the appearance of subsets of entangled factor variables in the intended tasks. Recent efforts along this line of work, includes unsupervised learning methods that exploit the enormous amounts of data available without the requirement of labels for each generating factor. Among the most popular methods includes β -VAE [15], Annealed VAE [16], Factor VAE [17], DIP-VAE [18] all imposing specific structure in the latent prior through modifications of the KL term. The β -VAE [15] for example includes a β scalar that controls the strength enforcing the latent prior. Increasing this scalar promotes the structure of the prior at the cost of divergence from the true marginal likelihood, thus β being a balancing term. Rooted in the concept of model identifiability, [13] however, challenged the line of work of unsupervised learning disentanglements as impossible.

Weakly-supervised learning methods on the other hand have exploited weak-labels as they have shown to facilitate some form of disentanglement. [19] proposes a method that consists in learning representations explaining the causal data generation mechanisms by promoting invariance to augmented data transformations, this under the principle of independent causal mechanism [20, 21]. Invariant risk minimization (IRM) of [22] seeks for representations that produce predictions invariant to environment contexts. [23] seeks to learn representations by grouped observations (i.e., a factor of variation shared between observations within a group) and proposes a multi-level VAE for learning group representations and tackle the limitations of VAE's assuming i.i.d observations. [24] shows that disentangled representations can be obtained under weak-supervision when pairs of measurements share a factor of variation. Their approach modifies the β -VAE objective by enforcing similarities between the shared generative factors of variation and a decoupling of those uncommon. Worth noting is [25], whose findings depict the method's capability to also disentangle when training in datasets constructed by unknown correlations between the generative factors (i.e., at least two factors that vary together) while being independent; a problem known to be one of the root causes affecting DL OOD robustness and fairness [8]. Identifiable VAE (iVAE) [6] proposes a method enabling a weak-form of model identification. The definition therein consists in finding models that for all $\mathbf{x}, \mathbf{z}, \forall \theta, \theta' : p_\theta(\mathbf{x}) = p_{\theta'}(\mathbf{x})$; in other words, find distinct θ and θ' for which the marginal data distributions are equal. This however, is done without using and testing [26] the constraints readable from the graphical generative model.

In light of these problems, the breadth of work in this research focuses towards contributing methods that seek to reconcile the issue of entanglement in existing deep representation learning models. The contributions of this work can be summarized as:

- “Regularization by Identification” (ReI) a modular regularization engine designed to align the behavior of large scale DL models with domain knowledge. Alignment criteria is anchored in causal identification analysis of directed acyclic graphs (DAG's), which, clearly stipulates the generative model assumed and advertises the conditions required for identification from observations valid under the DAG model. Derivation of ReI in a given learning problem applies the rules of the *do*-calculus of [27] to delete, exchange actions for observations and provide the adjustments necessary to guarantee identification of the involved causal relationships from observational data.
- We show under a pre-specified DAG model G encoding the typical data generative process used in the disentanglement works of [15, 12, 17], that standard representation learning frameworks present collider bias behaviour; a type of bias producing entanglement between the effects of the generating factors. An issue which has been either overlooked or not looked at all in representation learning to the best of our knowledge. For this, we reformulate the representation learning problem from a variational inference standpoint and derive under ReI the conditions that guarantee identification and that ultimately produce disentanglement.

- Provide empirical evidence that shows the potential of ReI in a dataset with joint variability between the generating factors; an issue recognized by [25] as the problem of correlated data. In this case, ReI offers the potential to produce representations that: (1) disentangle the effects of the generating factors with results well aligned with true expected behavior (e.g., from like physics principles) supporting interpretation and understanding and (2) are more generalizable in the presence of out-of-distribution examples in comparison to the standard non-identifiable DL model counterparts.

2 Approach

2.1 Generative Model

Consider the problem of approximate posterior $p(\mathbf{z}|\mathbf{x}, \mathbf{y}_c)$ inference as in the VAE framework of [5], with the distinction that unknown latent variable \mathbf{z} is conditioned on a generative factor \mathbf{y}_c . Measurements $\{\mathbf{x}^{(i)}\}_{i=1}^N$ are drawn from the marginal data distribution $p(\mathbf{x})$ generated by factor variables \mathbf{y} which admits factorizations of the form $p(\mathbf{y}) = \prod_c p(\mathbf{y}_c)$. The true posterior $p(\mathbf{z}|\mathbf{x}, \mathbf{y}_i)$ has powerfull representational properties that if well approximated, can produce disentangled representations, remove potential sources of undesired spurious correlations, with better generalization possibilities to OOD cases while also provide clear paths for explaining and understanding the effects of the underlying generative mechanisms, a much needed requirement for scientific discovery.

In the variational inference framework this generative model can be encoded by the directed acyclic graph (DAG) G in Fig.1.

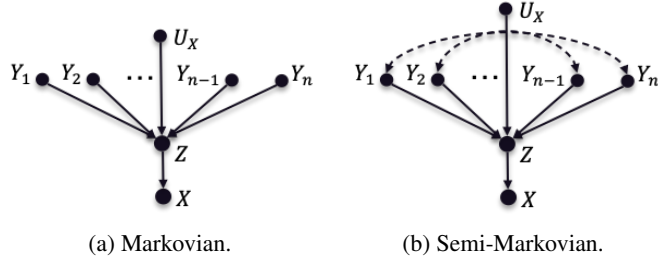


Figure 1: DAG G encoding generative process.

Variable $\mathbf{x} \in \mathbb{R}^M$ represents the sensor measurements, $\mathbf{y} \in \mathbb{R}^n$ with elements $\mathbf{y}_c, c \in \{1, \dots, n\}$ are the ground truth generating factors (e.g., class membership scores), respectively. Sensor noise is denoted by the unmeasured $\mathbf{u}_x \in \mathbb{R}^M$ and $\mathbf{z} \in \mathbb{R}^M$ is a learned latent representation. Arrows emanating from \mathbf{y}_c to \mathbf{z} , \mathbf{z} to \mathbf{x} are aligned with the causality of the generation mechanisms. In other words, there is causal prescedence of the \mathbf{y}_c 's and they are a direct cause (i.e., implied by the direct arrows between variables) of \mathbf{z} . Inspection of Fig. 1 reveals potential problems with the connections $\mathbf{y}_c \rightarrow \mathbf{z} \leftarrow \mathbf{y}_j$ with $j \neq c$, indicative of a collider [28, 29, 26]; a source of potential bias. This bias occurs when two or more independent variables have a direct causal influence on a variable (i.e., a collider) as they will become correlated when conditioning (e.g., observing) the colliding variable. This spurious correlation between \mathbf{y}_c and \mathbf{y}_j can be a source of bias. For example, consider the case of $Y = X + Z$ with X and Z independent. When variable Y is conditioned (e.g., $Y = 4$) variables X and Z become correlated by this restriction. This collider bias phenomenon occurs as information on one of the causes makes the other causes involved more or less likely given that the consequence has occurred; even when the causes are independent [27]. In the variational framework, training by enforcing the likelihood term $p(\mathbf{x}|\mathbf{z})p(\mathbf{z}|\mathbf{y}_c)$ will, we argue open the free flow of information between the colliding generating factors \mathbf{y}_c producing entangled representations if it remains untreated. Related works based on variational inference fundamentals like the VAE [5] and even the supervised conditional VAE [30] are susceptible to this collider problem when conditioning on \mathbf{z} as required by the likelihood function as no adjustment for the collider is provided. We recognize this as an important issue here and provide possible avenues for its resolution via the ReI framework while also providing connections to extend some of the analysis in identifiable based learning methods [15, 24, 25] to integrate ReI in a modularized fashion.

2.2 Identification of Causal Effect Relationships

Identification here sticks to Pearl’s causal analysis framework [26] to control/adjust for potential sources of bias (e.g., confounding, collider bias) between the participating variables. A DAG G [27] (see Appendix) encodes domain knowledge of the data generation mechanisms serves as a graphical tool to formulate the adjustments necessary for identification to control for bias or the free flow of information between variables with causally-unsupported dependencies. Identification of a causal relationship $p(y|\hat{x}) = p(y|do(X = x))$ enables inference of an intervention $do(X = x)$ from observed quantities alone and a model DAG G . Deriving such identifyability enables estimation of the quantities of interest unambiguously as G provides the model under which the distribution holds [27]. This, unlike nonidentifiable quantities which can only be defined ambiguously, and are likely to produce entangled representations. The VAE framework known to be very effective in approximating the marginal data distribution $p(\mathbf{x})$ does not provide any identifiable guarantees on the posterior distribution, rendering latent representations meaningless (in the sense of providing information about the true generative factors or its effects). Alternatively, the breadth of recent work most successful in representation disentanglement of the generative factors has relied in some form of identification [20, 23, 19, 24, 6, 25].

In light of this discussion, we seek to lift the conventional usage of the approximate posterior $q(\mathbf{z}|\mathbf{x})$ in the VAE framework, for the causal relationship $p(\mathbf{z}|\mathbf{x}, \hat{\mathbf{y}}_c)$ invoking intervention quantities of the $do(\mathbf{Y}_c = \mathbf{y}_c)$. Inspection of the assumed DAG G model in Fig.1 adverts the presence of a collider. Adjustment for the participating variables in this collider is resolved by identification of the causal relationship $p(\mathbf{z}|\hat{\mathbf{y}}_c)$ involved in the derivation of the posterior. This later (see Appendix for full derivation) is given in Eq.(1) as:

$$p(\mathbf{z}|\hat{\mathbf{y}}_c) = \sum_{\mathbf{w}_c} p(\mathbf{z}|\mathbf{y})p(\mathbf{w}_c) = \mathbb{E}_{p(\mathbf{w}_c)} [p(\mathbf{z}|\mathbf{y})] \quad (1)$$

where for easy of exposition, we denote the generating factors in the system outside of \mathbf{y}_c by the set $\mathbf{w}_c = \{\mathbf{y}_j : j \neq c\}$, with $\mathbf{y} = \mathbf{w}_c \cup \{\mathbf{y}_c\}$. Note that the right hand side of Eq. (1) includes terms involving only standard probabilities obtained from observations. These as Eq.(1) implies can be computed by the expectation over the generating factors \mathbf{w}_c of the conditional latent distribution.

Leaving one of the participating variables without control while conditioning on a collider unblocks the flow of information across the paths colliding at the common consequence. In the case of Fig.1 for example, the relationship $p(\mathbf{z}|\hat{\mathbf{u}}_x)$ is unidentified as the factor \mathbf{u}_x is unmeasured and so the adjustment of Eq.(1) is not possible. Bias from the unmeasured \mathbf{u}_x under model G of Fig.1 in the causal queries $p(\mathbf{z}|\hat{\mathbf{y}}_c)$ will result in entanglement with the effects of $p(\mathbf{z}|\hat{\mathbf{u}}_x)$. Alternative remedies are in existence to mitigate this problem, but these have to rely on a parametrization enabling some form of approximation to $p(\mathbf{z}|\hat{\mathbf{u}}_x)$. When \mathbf{u}_x represents sensor noise for example, assumed to be stationary and uncorrelated with \mathbf{y} as depicted in the DAG model G of Fig.1, possibilities like the denoising methods of [31, 32] exist, which have shown to be highly effective.

2.3 Regularization by Identification

Regularization by identification (ReI) is a regularization engine defined by identification of the causal queries involved in the learning problem. Key step is that identification of the causal queries is anchored in analysis of a pre-specified DAG G model encoding the particular data generation mechanisms under which the identifications are valid. ReI reformulates traditional learning frameworks to make the necessary adjustments for causal identification of the involved queries; made explicit by regularization. This altogether different from the weakly-supervised setting of [19, 21, 22] which aim at finding the generating mechanisms by imposing some form of invariance to real or augmented data variability. Or to [23, 24] imposing invariance to shared generative factors between at least pairs of observations while keeping those detected as varying, free. In addition, distinct from [6], our method relies on identification of the causal queries valid under a specified DAG G model rather than a statistical notion of model identification. Lastly, throughout this work the latent space lives in the same space as the observations (this made without restriction of analysis to latents living in lower dimensional spaces). This characteristic made in similarity with inverse denoising problems [33, 31] and denoising diffusion models [34, 35] as examples. We assume this to yield representations more suitable to support interpretation, explanation and understanding of the effects of generating factors on data; as later verified empirically in Section 3.2.

The learning problem of the variational framework of [5] optimizes the evidence lower bound (ELBO) to approximate the true posterior $p^*(\mathbf{z}|\mathbf{x})$ given measurements $\{\mathbf{x}^{(i)}\}_{i=1}^N$. The ELBO can be formulated by two terms: a likelihood $\mathcal{L}_\ell(\theta, \phi; \mathbf{x}^{(i)})$ and a regularizer $\mathcal{L}_\rho(\theta, \phi; \mathbf{x}^{(i)})$ as:

$$\mathcal{L}(\theta, \phi; \mathbf{x}^{(i)}) = \mathcal{L}_\ell(\theta, \phi; \mathbf{x}^{(i)}) - \lambda \mathcal{L}_\rho(\theta, \phi; \mathbf{x}^{(i)}) \quad (2)$$

where the likelihood term of most VAE flavors out there is given by Eq.(3) as:

$$\mathcal{L}_\ell(\theta, \phi; \mathbf{x}^{(i)}) = \mathbb{E}_{q(\mathbf{z}|\mathbf{x}^{(i)})} \left[\log p(\mathbf{x}^{(i)}|\mathbf{z}) \right] \quad (3)$$

and the regularizer $\mathcal{L}_\rho(\theta, \phi; \mathbf{x}^{(i)})$ given in case of the standard VAE by the Kullback-Leibler (KL) divergence

$$\mathcal{L}_\rho(\theta, \phi; \mathbf{x}^{(i)}) = D_{KL}(q(\mathbf{z}|\mathbf{x}^{(i)}) || p(\mathbf{z})) \quad (4)$$

imposing a prior $p(\mathbf{z})$, typically a standard Gaussian, on the approximate posterior. The θ, ϕ are the parameters of the encoder and decoder models, respectively, and optimized over the training dataset. The scalar λ in Eq.(2) is the regularizer strength balancing tradeoffs between the likelihood and priors, a parameter utilized by the β -VAE to promote the prior structure. Other extensions without identification guarantees, structuring the latent space by class under supervision is the conditional VAE of [30] approximating instead, the conditional posterior $p(\mathbf{z}|\mathbf{x}, \mathbf{y})$ given data pairs $\{\mathbf{x}^{(i)}, \mathbf{y}^{(i)}\}_{i=1}^N$.

ReI reformulates the VAE, CVAE by lifting as in Section 2.2 the posterior $p(\mathbf{z}|\mathbf{x}, \mathbf{y})$ to the causal relationship $p(\mathbf{z}|\mathbf{x}, \hat{\mathbf{y}}_c)$. The reformulated posterior adjusted to render it identifiable under DAG G in Fig.1 is equivalent to:

$$p(\mathbf{z}|\mathbf{x}, \hat{\mathbf{y}}_c) = p(\mathbf{x}|\mathbf{z}) \mathbb{E}_{p(\mathbf{w}_c)} [p(\mathbf{z}|\mathbf{y})] / p(\mathbf{x}, \mathbf{y}_c) \quad (5)$$

involving the observables $\{\mathbf{x}^{(i)}, \mathbf{y}^{(i)}\}_{i=1}^N$. The adjustments in Eq.(5) block the flow of information between variables $\mathbf{y}_c \rightarrow \mathbf{z} \leftarrow \mathbf{w}_c$ when conditioning on \mathbf{z} , as required by the variational framework. The full derivation of Eq.(5) showing it an identifiable quantity can be referred to in the Appendix.

The adjustment of the ELBO made to reflect the causal relationship $p(\mathbf{z}|\mathbf{x}, \hat{\mathbf{y}}_c)$ instead of the standard posterior $p(\mathbf{z}|\mathbf{x}, \mathbf{y}_c)$. Derived in the Appendix, the adjustments required for identification of $p(\mathbf{z}|\mathbf{x}, \hat{\mathbf{y}}_c)$ results in the reformulated regularizer of the ELBO given in Eq.(6) as:

$$\mathcal{L}_\rho(\theta, \phi; \mathbf{x}^{(i)}, \mathbf{y}^{(i)}) = D_{KL} \left(q(\mathbf{z}|\mathbf{x}^{(i)}, \mathbf{y}_c^{(i)}) || \mathbb{E}_{p(\mathbf{w}_c)} [p(\mathbf{z}|\mathbf{y}^{(i)})] \right) \quad (6)$$

Note that the necessary adjustments that render the causal relationship identifiable imposes constraints only on the ELBO regularizer. The likelihood function in learning problems remains, at least to the best of our knowledge, without modification in general. This is also consistent with the causal literature [36, 26] where free parameters abide to the likelihood function (e.g., least squares) while the adjustments imposed by identification constrain it (e.g., to be zero in the case of linear models [37]). Given these characteristics, we term our method ReI; as the constraints required to make the causal queries involved in the learning problem identifiable can be directly imposed by a regularizer. One of the motivating characteristics of ReI observed in the aforementioned reformulation of the ELBO is its modularity. This enables, the constraints imposed by ReI, like the regularizer derived in the VAE reformulation be added in a plug and play manner to other frameworks like [15, 12, 17, 23, 24] similar to the work of [38] this last one focusing on regularizing denoisers.

In terms of the functional encoder/decoder approximators, deep model capacity is assumed to satisfy the data processing inequality with equality constraints. In other words, the mutual information I between \mathbf{Y}_c and \mathbf{Z} is preserved relative to \mathbf{Y}_c and \mathbf{X} (i.e. $I(\mathbf{Y}_c, \mathbf{Z}) = I(\mathbf{Y}_c, \mathbf{X})$). This assumption has been used in other works [24, 39] and justified in the VAE's objective to faithfully approximate the marginal data distribution.

3 Experimentation

Experiments were conducted in applications of spectroscopic sensors, specifically using data from a laser induced breakdown spectroscopy (LIBS) instrument. LIBS is a remote sensing technology used for prediction of the chemical composition of geomaterials (e.g., rocks, soil) based on its

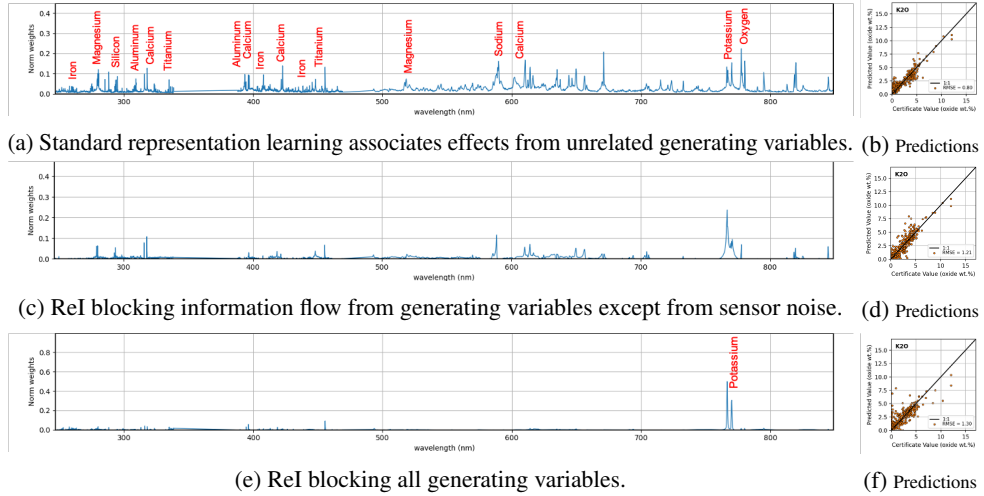


Figure 2: Comparison of the learned representations for chemical oxide K₂O.

signatures. On Mars, the ChemCam/SuperCam LIBS based instruments are capable of investigating < 1mm size samples by laser excited samples from up to 7m distances. It is equipped with a 1064nm laser and ultraviolet (UV), visible (VIO) and near infrared (NIR) band spectrometers; which altogether are capable of collecting the sample’s spectral signatures occurring between 240-905nm. It is through the analysis of such spectral signatures that chemical composition information of a sample can be readily extracted. Focus here, is applying the ReI framework directed towards three tasks: (1) representation disentanglement, (2) prediction and (3) transfer. First one consists in learning representations that characterize the spectral signatures of specific chemical elements. Second, uses the learned representations to predict chemical content of sampled materials while the third tests the generalization capabilities to dataset shifts by training from data collected in a controlled laboratory setting on Earth while deployment occurs in the wild on the Martian surface.

3.1 Dataset

The ChemCam LIBS instrument [40] datasets contain raw and denoised spectra obtained from a variety of targets (e.g., rocks, soil) and from reference calibration standards of known and certified chemical composition. The specific datasets we employ consists of spectrally resolved LIBS signal measurements collected on Earth in a laboratory setting from a set of ~ 585 reference calibration standards [41] and on Mars from a set of 10 reference standards of known true composition. Each target is repeatedly shot (e.g., 50 times) following each time measurements of the full 240-905 nm LIBS signal. After collection, wavelengths within the bands [240.811, 246.635], [338.457, 340.797], [382.13, 387.859], [473.184, 492.427], [849, 905.574] were ignored out consistent with practices of the ChemCam team [41].

3.2 Representation disentanglement

The abilities of ReI for learning disentangled representations were evaluated here. Training utilizes example pairs $\{\mathbf{x}^{(i)}, \mathbf{y}^{(i)}\}_{i=1}^N$ of LIBS signal \mathbf{x} measurements and corresponding chemical composition scores ground truth \mathbf{y} . Scores \mathbf{y}_c represent % oxide composition for $c \in \{1, \dots, 11\}$ indexing $\{\text{SiO}_2, \text{TiO}, \text{Al}_2\text{O}_3, \text{FeO}_T, \text{MgO}, \text{MnO}, \text{CaO}, \text{Na}_2\text{O}, \text{K}_2\text{O}, \text{CO}_2, \text{H}_2\text{O}\}$ and which altogether with sensor noise $\mathbf{u}_x \in \mathbb{R}^M$, produces the measured LIBS signal $\mathbf{x} \in \mathbb{R}^M$ with $M = 5485$.

For this, qualitative comparative evaluations of the produced representations from our ReI framework were performed in light of the known characteristic spectral response of each chemical oxide. We trained the VAE in an MLP architecture to produce representations which are compared in three cases: (1) the standard unidentified (causally-unconstrained), (2) constrained by ReI as in Eq.(2) with generating factors identified except for sensor noise \mathbf{u}_x and (3) ReI with all generating factors identified. Training uses the 585 reference calibration targets under leave one out while testing was done on data from the standard left out until all targets are covered. Hyperparameters of the DL

model were set to an initial lr of 1.0, decayed after 75 epochs with cosine annealing [42] and with #epochs 300. Batches were constructed at each epoch from a set of 64 shot-averaged examples randomized over the whole training set without replacement. The shot-averages are computed by averaging the LIBS signal representations over an individual target and laser shot location. This averaging is consistent with common practices of the ChemCam team [43, 41]. From a practical standpoint, regularization by ReI in Eq.(6) requires computing expectation over distributions of the generative factors. This is computationally intractable and we resorted to approximations by sampling with a limited number of samples (throughout the experiments with spectral data we used a 1000 samples) per causal relationship. This approximation resulted in some information leaks from other generating variables. This phenomenon can be observed qualitatively for example in the small peaks present in Fig.2c (from 200-500nm wavelengths).

A representative example on the learned representations corresponding to chemical oxide K_2O is shown in Fig.2. These were generated by sampling from $q(\mathbf{z}|\mathbf{x}^{(i)}, \mathbf{y}_c^{(i)})$ by querying \mathbf{y}_c as K_2O and averaging over $L = 100$ samples. Figs.2a, 2c and 2e shows the learned representations for K_2O in: (1) standard causally-unconstrained, (2) ReI with sensor noise \mathbf{u}_x unidentified and (3) ReI with identification of all generating factors. The vertical axis of each plot shows the normalized magnitude and the horizontal axis represents spectral wavelength importance. Figs.2b, 2d and 2f illustrate the corresponding prediction performance \tilde{y}_c of the three cases using the representations \mathbf{z} along with a trained linear prediction head. Prediction performance by looking into point distribution along the 1:1 line and as measured by the root mean squared error (RMSE) shows similar performances in all three cases; with a marginal advantage of the standard VAE (i.e., (1) 0.8, (2) 1.21, (3) 1.30). However, these all come from distinct learned representations with key observations supporting evidence of collider behavior. First, note that K_2O (Potassium oxide) is known and expected to respond to wavelengths around $\sim 770\text{nm}$ as labeled Fig.2a illustrating the ground truth expected spectral responses of a variety of chemical elements. The standard VAE in Fig.2a resulted in a representation with spectral peaks deemed important spread throughout the entire spectrum. This is indicative of information flow between the generative causes $\mathbf{w}_c = \{\mathbf{y}_j : j \neq c\}$ outside of \mathbf{y}_c (i.e., K_2O) to \mathbf{y}_c from the unblocked paths $\mathbf{w}_c \rightarrow \mathbf{z} \leftarrow \mathbf{y}_c$ occurring when conditioning on \mathbf{z} or its descendant \mathbf{x} . Fig.2c in contrast shows the resulting representation obtained by ReI with all generative factors except for sensor noise \mathbf{u}_x identified. Although most of the wavelengths previously deemed important were flattened, some spectral peak patterns from Fig.2a still persist although at a lower scale. This, we argue is indicative of the paths $\mathbf{w}_c \rightarrow \mathbf{z} \leftarrow \mathbf{u}_x$ and $\mathbf{u}_x \rightarrow \mathbf{z} \leftarrow \mathbf{y}_c$ producing information bridges between these variables. Finally, Fig.2e illustrates the representation by ReI with all generative factors identified. Note that in this case, most wavelengths were brought down to zero except for the two strong peaks at $\sim 770\text{nm}$. This, in alignment with the expected characteristic spectral response for K_2O as labeled therein. Identification of the causal relationships involved in the learning variational framework thus produced representations well aligned with the expected effects of the generating factors.

Empirical evidence provided thus supports our claim that DL models ill-suffer from collider bias. Although, as presented here in the prediction of in-distribution examples, downstream tasks can obscure the aforementioned illness, the task of representing the effects of generating factors; clearly shows evidence of this problem, with effects supporting collider behavior. These findings, thus provide a plausible alternative explanation to the spurious association problems between factors found in [44, 45, 46, 47], to fairness [48], and provide a venue for analysis and remediation through causality as viewed by [49] and tackled here by ReI. We would like to note also that the learned representations from ReI visualized pictorially are amenable for interpretation, explain the effects of generating factors as they relate to the effects of the measuring apparatus, and can support understanding much needed for scientific discovery.

3.3 Prediction and Transfer

Quantitative evaluations that compared generalization in the prediction tasks of chemical composition of the learned representations in the presence of dataset shifts are evaluated here. The problem of dataset shifts originate within the scope of the LIBS application by training from data collections of LIBS measurements from targets on Earth in a laboratory setting while deployment occurs in data collections in the wild from Mars. [41] found that the Martian environment has effects that shift the distribution of measurements in relationship to those on Earth and provided a manual engineered

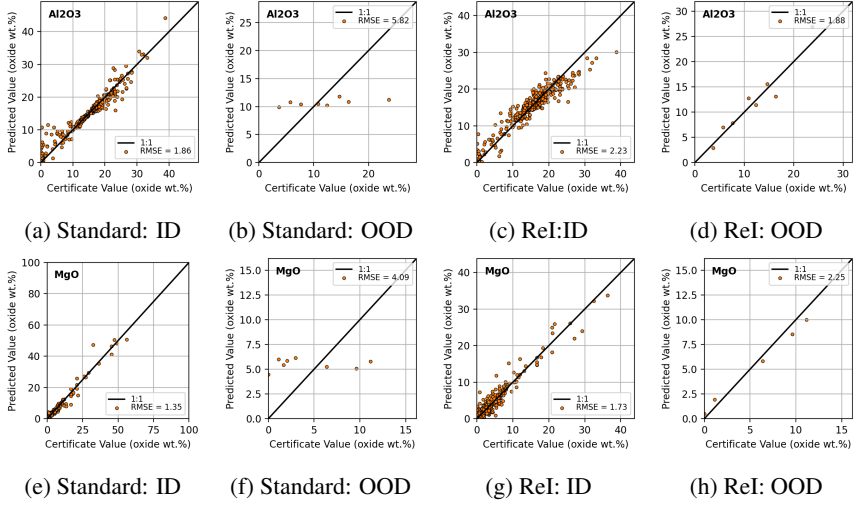


Figure 3: Performance comparison of the learned representations in out-of-distribution transfer.

Table 1: Transfer Performance Comparison

Architecture	RMSE (% oxide)
FC(10)	5.19
MLP(10)	5.06
MLPMixer(8)	5.23
ResNet(18) + FC(10)	6.23
U-Net +FC(5)	5.12
Transformer + FC(10)	6.12
VAE + FC(10)	4.51
β -VAE +FC(10)	4.13
F-VAE +FC(10)	4.01
DIP-VAE +FC(10)	4.67
ReI-VAE+FC(1)	2.45

approach for its correction. This task then seeks to investigate the transferability of the representations in the presence of out-of-distribution shifts caused by deployment in a distinct environment.

Example representative results were included in Fig.3 which show ground truth versus prediction plots for two element oxides Al_2O_3 and MgO . Four leftmost Figs.3a,3e,3b,3f corresponds to performance results of the learned representation using standard VAE+FC linear head whereas the rightmost four Fig.3c,3g,3d,3h shows those from ReI. Figs. 3a,3e,3c,3g show that both standard and ReI present similar performance for in distribution example testing (under leave one out), with the standard being marginally better in RMSE. In contrast, Figs.3b,3f,3c,3g shows significant differences in performance for out-of-distribution (OOD) example testing. ReI presents better behaved performance and outperforms by larger margins compared to the standard in all cases. Note that even though the standard methods present a performance advantage over ReI for in-distribution examples, that this is not the case for out-of-distribution examples collected in the wild from Mars. ReI learns representations with disentangled variables that show better generalizations against the tested out-of-distribution examples. This behavior, consistant with findings by [50] showing that highly predictive non-robust features in the data tend to reduce learner performance when presented with out-of-distribution examples.

3.4 DL model architectures at transfer

Table 1 provides addditional results comparing performance on Earth-to-Mars transfer on a variety of DL architectures and averaged over all elements $y \in \mathbb{R}^n$ with $n = 11$. Comparisons include fully connected (FC), multilayer perceptron (MLP), MLP Mixer [51], ResNet [52], U-Net [53],

Transformers [54], VAE [5], Beta-VAE [15], Factor-VAE [17], DIP-VAE [18]. Note that some of the architectures do not produce a latent representation explicitly, these are however rather trained end-to-end for prediction. The number in parenthesis next to each architecture name (e.g., FC(10)) expresses the corresponding depth of layers. The results of Table 1 show that ReI outperforms standard architectures in cases of OOD examples regardless of the inductive biases implied by the architectural designs in comparison. The unsupervised representation learning methods Beta-VAE, factorized VAE and DIP-VAE trained with a supervised prediction loss performed better at transfer than the standard deep learning architectures compared. However, ReI explicitly and directly incorporating information (e.g., their presence and interaction) about the data generative factors and controlling for the effects of correlations between these was able to outperform them all. Fig.4 shows instead transfer performance as a function of DL model depth. In this case, the FC, MLP, MLPmixer and ResNet+FC networks were compared. This plot shows that ReI is capable of outperforming standard DL models which did not exhibit generalization capabilities to OOD cases regardless of depth in this case. As a remark

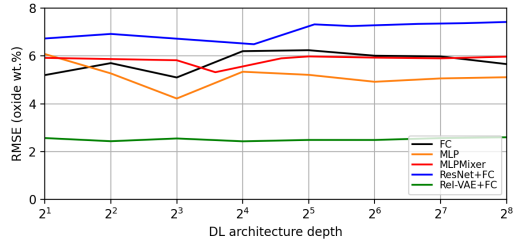


Figure 4: Transfer performance versus DL model depth.

we would like to highlight that gains in task performance may not necessarily translate into more generalizable DL models. In fact, as evidenced by experiments, these may sometimes trick one's belief of a better model. In our case, these issues were settled through experiments evaluating the resulting representations of the effects between the generating factors and the measuring apparatus and the expectations from domain knowledge. Finally, we would like to highlight some of the limitations of this work. ReI requires full derivation of the specific identifiability conditions of the particular data generation process of the dataset when this does not hold with that of Fig.1. This human exercise of modeling the generation process through DAGs and deriving the identifiability conditions (using the rules of do-calculus) involved in the learning problem for the specified DAG can be time consuming. Discovering models of the generation process automatically [55] is an active area of research but this is outside the scope of this work. In some cases, identifiability conditions for a given DAG can be more challenging to obtain or does not exist due to the presence of unobserved variables requiring control. Measurable proxies can be exploited as in [56] in some of these cases, but in some others where this is not possible one has to resort to parametrization approximations which may result in entanglements of residuals between the true and sampled parametrized distributions; this, of course without identification guarantees. In the example application of chemical composition from LIBS we discussed this issue in the case of the sensor noise variable and shown in Fig. 2c.

4 Conclusions

In this work, we proposed ReI: a regularization method that aligns DL models to domain knowledge by leveraging the DAG. We argued that standard non-identifiable DL models are ill-biased by collider behaviour and showed supporting empirical evidence of this. In a variational framework, we showed how analysis of the graphical data generative model under the lens of causality can be used to adjust for collider bias via ReI in representation learning problems. Empirical evidence shows ReI is capable of learning the effects between the individual generating factors and the sensor, removing collider bias, producing representations in disentangled form, generalizable to OOD example cases and supporting interpretation, explanation and understanding of both factor effects and manipulations of these for sampling posterior generation.

References

- [1] Claude Elwood Shannon, “A mathematical theory of communication,” *The Bell system technical journal*, vol. 27, no. 3, pp. 379–423, 1948.
- [2] Karl Pearson, “Liii. on lines and planes of closest fit to systems of points in space,” *The London, Edinburgh, and Dublin philosophical magazine and journal of science*, vol. 2, no. 11, pp. 559–572, 1901.
- [3] Karl Pearson, “Liii. on lines and planes of closest fit to systems of points in space,” *The London, Edinburgh, and Dublin philosophical magazine and journal of science*, vol. 2, no. 11, pp. 559–572, 1901.
- [4] Anthony J Bell and Terrence J Sejnowski, “An information-maximization approach to blind separation and blind deconvolution,” *Neural computation*, vol. 7, no. 6, pp. 1129–1159, 1995.
- [5] Diederik P Kingma and Max Welling, “Auto-encoding variational bayes,” *arXiv preprint arXiv:1312.6114*, 2013.
- [6] Ilyes Khemakhem, Diederik Kingma, Ricardo Monti, and Aapo Hyvärinen, “Variational autoencoders and nonlinear ica: A unifying framework,” in *International Conference on Artificial Intelligence and Statistics*. PMLR, 2020, pp. 2207–2217.
- [7] Brenden M Lake, Tomer D Ullman, Joshua B Tenenbaum, and Samuel J Gershman, “Building machines that learn and think like people,” *Behavioral and brain sciences*, vol. 40, 2017.
- [8] Alexander D’Amour, Katherine Heller, Dan Moldovan, Ben Adlam, Babak Alipanahi, Alex Beutel, Christina Chen, Jonathan Deaton, Jacob Eisenstein, Matthew D Hoffman, et al., “Underspecification presents challenges for credibility in modern machine learning,” *Journal of Machine Learning Research*, 2020.
- [9] Christian Szegedy, Wojciech Zaremba, Ilya Sutskever, Joan Bruna, Dumitru Erhan, Ian Goodfellow, and Rob Fergus, “Intriguing properties of neural networks,” *arXiv preprint arXiv:1312.6199*, 2013.
- [10] Judea Pearl, “The seven tools of causal inference, with reflections on machine learning,” *Commun. ACM*, vol. 62, no. 3, pp. 54–60, Feb. 2019.
- [11] Yoshua Bengio, Aaron Courville, and Pascal Vincent, “Representation learning: A review and new perspectives,” *IEEE transactions on pattern analysis and machine intelligence*, vol. 35, no. 8, pp. 1798–1828, 2013.
- [12] Irina Higgins, David Amos, David Pfau, Sébastien Racanière, Loïc Matthey, Danilo Rezende, and Alexander Lerchner, “Towards a definition of disentangled representations,” *arXiv preprint arXiv:1812.02230*, 2018.
- [13] Francesco Locatello, Stefan Bauer, Mario Lucic, Gunnar Raetsch, Sylvain Gelly, Bernhard Schölkopf, and Olivier Bachem, “Challenging common assumptions in the unsupervised learning of disentangled representations,” in *international conference on machine learning*. PMLR, 2019, pp. 4114–4124.
- [14] Sjoerd Van Steenkiste, Francesco Locatello, Jürgen Schmidhuber, and Olivier Bachem, “Are disentangled representations helpful for abstract visual reasoning?,” *Advances in Neural Information Processing Systems*, vol. 32, 2019.
- [15] Irina Higgins, Loïc Matthey, Arka Pal, Christopher Burgess, Xavier Glorot, Matthew Botvinick, Shakir Mohamed, and Alexander Lerchner, “beta-vae: Learning basic visual concepts with a constrained variational framework,” 2016.
- [16] Christopher P Burgess, Irina Higgins, Arka Pal, Loïc Matthey, Nick Watters, Guillaume Desjardins, and Alexander Lerchner, “Understanding disentangling in beta-vae,” *arXiv preprint arXiv:1804.03599*, 2018.
- [17] Hyunjik Kim and Andriy Mnih, “Disentangling by factorising,” in *International Conference on Machine Learning*. PMLR, 2018, pp. 2649–2658.
- [18] Abhishek Kumar, Prasanna Sattigeri, and Avinash Balakrishnan, “Variational inference of disentangled latent concepts from unlabeled observations,” in *International Conference on Learning Representations*, 2018.

- [19] Jovana Mitrovic, Brian McWilliams, Jacob Walker, Lars Buesing, and Charles Blundell, “Representation learning via invariant causal mechanisms,” *arXiv preprint arXiv:2010.07922*, 2020.
- [20] Jonas Peters, Peter Bühlmann, and Nicolai Meinshausen, “Causal inference by using invariant prediction: identification and confidence intervals,” *Journal of the Royal Statistical Society: Series B (Statistical Methodology)*, vol. 78, no. 5, pp. 947–1012, 2016.
- [21] Jonas Peters, Dominik Janzing, and Bernhard Schölkopf, *Elements of causal inference: foundations and learning algorithms*, The MIT Press, 2017.
- [22] Martin Arjovsky, Léon Bottou, Ishaaan Gulrajani, and David Lopez-Paz, “Invariant risk minimization,” *arXiv preprint arXiv:1907.02893*, 2019.
- [23] Diane Bouchacourt, Ryota Tomioka, and Sebastian Nowozin, “Multi-level variational autoencoder: Learning disentangled representations from grouped observations,” in *Proceedings of the AAAI Conference on Artificial Intelligence*, 2018, vol. 32.
- [24] Francesco Locatello, Ben Poole, Gunnar Rätsch, Bernhard Schölkopf, Olivier Bachem, and Michael Tschannen, “Weakly-supervised disentanglement without compromises,” in *International Conference on Machine Learning*. PMLR, 2020, pp. 6348–6359.
- [25] Frederik Träuble, Elliot Creager, Niki Kilbertus, Francesco Locatello, Andrea Dittadi, Anirudh Goyal, Bernhard Schölkopf, and Stefan Bauer, “On disentangled representations learned from correlated data,” in *International Conference on Machine Learning*. PMLR, 2021, pp. 10401–10412.
- [26] Judea Pearl, *Causality*, Cambridge university press, 2009.
- [27] Judea Pearl, “Causal diagrams for empirical research,” *Biometrika*, vol. 82, no. 4, pp. 669–688, 1995.
- [28] Joseph Berkson, “Limitations of the application of fourfold table analysis to hospital data,” *Biometrics Bulletin*, vol. 2, no. 3, pp. 47–53, 1946.
- [29] JinHyung Kim and Judea Pearl, “A computational model for causal and diagnostic reasoning in inference systems,” in *International Joint Conference on Artificial Intelligence*, 1983, pp. 0–0.
- [30] Kihyuk Sohn, Honglak Lee, and Xinchen Yan, “Learning structured output representation using deep conditional generative models,” *Advances in neural information processing systems*, vol. 28, 2015.
- [31] Jaakko Lehtinen, Jacob Munkberg, Jon Hasselgren, Samuli Laine, Tero Karras, Miika Aittala, and Timo Aila, “Noise2noise: Learning image restoration without clean data,” *arXiv preprint arXiv:1803.04189*, 2018.
- [32] Samuli Laine, Tero Karras, Jaakko Lehtinen, and Timo Aila, “High-quality self-supervised deep image denoising,” *Advances in Neural Information Processing Systems*, vol. 32, 2019.
- [33] Kai Zhang, Wangmeng Zuo, Yunjin Chen, Deyu Meng, and Lei Zhang, “Beyond a gaussian denoiser: Residual learning of deep cnn for image denoising,” *IEEE transactions on image processing*, vol. 26, no. 7, pp. 3142–3155, 2017.
- [34] Jascha Sohl-Dickstein, Eric Weiss, Niru Maheswaranathan, and Surya Ganguli, “Deep unsupervised learning using nonequilibrium thermodynamics,” in *International Conference on Machine Learning*. PMLR, 2015, pp. 2256–2265.
- [35] Jonathan Ho, Ajay Jain, and Pieter Abbeel, “Denoising diffusion probabilistic models,” *Advances in Neural Information Processing Systems*, vol. 33, pp. 6840–6851, 2020.
- [36] Peter Spirtes, Thomas Richardson, Christopher Meek, Richard Scheines, and Clark Glymour, “Using d-separation to calculate zero partial correlations in linear models with correlated errors,” *Publisher: Carnegie Mellon University*, 1996.
- [37] Peter Spirtes, “Directed cyclic graphical representations of feedback models,” in *Proceedings of the Eleventh conference on Uncertainty in artificial intelligence*, 1995, pp. 491–498.
- [38] Singanallur V Venkatakrishnan, Charles A Bouman, and Brendt Wohlberg, “Plug-and-play priors for model based reconstruction,” in *2013 IEEE Global Conference on Signal and Information Processing*. IEEE, 2013, pp. 945–948.
- [39] Chengzhi Mao, Kevin Xia, James Wang, Hao Wang, Junfeng Yang, Elias Bareinboim, and Carl Vondrick, “Causal transportability for visual recognition,” in *Proceedings of the IEEE/CVF Conference on Computer Vision and Pattern Recognition*, 2022, pp. 7521–7531.

[40] Roger C Wiens, Sylvestre Maurice, Bruce Barraclough, Muriel Saccoccio, Walter C Barkley, James F Bell, Steve Bender, John Bernardin, Diana Blaney, Jennifer Blank, et al., “The chemcam instrument suite on the mars science laboratory (msl) rover: Body unit and combined system tests,” *Space science reviews*, vol. 170, no. 1, pp. 167–227, 2012.

[41] Samuel M Clegg, Roger C Wiens, Ryan Anderson, Olivier Forni, Jens Frydenvang, Jeremie Lasue, Agnes Cousin, Valerie Payre, Tommy Boucher, M Darby Dyar, et al., “Recalibration of the mars science laboratory chemcam instrument with an expanded geochemical database,” *Spectrochimica Acta Part B: Atomic Spectroscopy*, vol. 129, pp. 64–85, 2017.

[42] Ilya Loshchilov and Frank Hutter, “SGDR: Stochastic gradient descent with warm restarts,” in *International Conference on Learning Representations*, 2017.

[43] R.C. Wiens, S. Maurice, J. Lasue, O. Forni, R.B. Anderson, S. Clegg, S. Bender, D. Blaney, B.L. Barraclough, A. Cousin, L. Delflores, D. Delapp, M.D. Dyar, C. Fabre, O. Gasnault, N. Lanza, J. Mazoyer, N. Melikechi, P.-Y. Meslin, H. Newsom, A. Ollila, R. Perez, R.L. Tokar, and D. Vaniman, “Pre-flight calibration and initial data processing for the chemcam laser-induced breakdown spectroscopy instrument on the mars science laboratory rover,” *Spectrochimica Acta Part B: Atomic Spectroscopy*, vol. 82, pp. 1 – 27, 2013.

[44] Ben Glocker, Robert Robinson, Daniel C Castro, Qi Dou, and Ender Konukoglu, “Machine learning with multi-site imaging data: An empirical study on the impact of scanner effects,” *arXiv preprint arXiv:1910.04597*, 2019.

[45] Robert Geirhos, Jörn-Henrik Jacobsen, Claudio Michaelis, Richard Zemel, Wieland Brendel, Matthias Bethge, and Felix A Wichmann, “Shortcut learning in deep neural networks,” *Nature Machine Intelligence*, vol. 2, no. 11, pp. 665–673, 2020.

[46] Mohammad Pezeshki, Oumar Kaba, Yoshua Bengio, Aaron C Courville, Doina Precup, and Guillaume Lajoie, “Gradient starvation: A learning proclivity in neural networks,” *Advances in Neural Information Processing Systems*, vol. 34, 2021.

[47] Imon Banerjee, Ananth Reddy Bhimireddy, John L Burns, Leo Anthony Celi, Li-Ching Chen, Ramon Correa, Natalie Dullerud, Marzyeh Ghassemi, Shih-Cheng Huang, Po-Chih Kuo, et al., “Reading race: Ai recognises patient’s racial identity in medical images,” *arXiv preprint arXiv:2107.10356*, 2021.

[48] Jieyu Zhao, Tianlu Wang, Mark Yatskar, Vicente Ordonez, and Kai-Wei Chang, “Men also like shopping: Reducing gender bias amplification using corpus-level constraints,” in *Proceedings of the 2017 Conference on Empirical Methods in Natural Language Processing*, 2017, pp. 2979–2989.

[49] Judea Pearl, “On measurement bias in causal inference,” in *Proceedings of the Twenty-Sixth Conference on Uncertainty in Artificial Intelligence*, Arlington, Virginia, United States, 2010, UAI’10, pp. 425–432, AUAI Press.

[50] Dimitris Tsipras, Shibani Santurkar, Logan Engstrom, Alexander Turner, and Aleksander Madry, “Robustness may be at odds with accuracy,” in *International Conference on Learning Representations*, 2018.

[51] Ilya O Tolstikhin, Neil Houlsby, Alexander Kolesnikov, Lucas Beyer, Xiaohua Zhai, Thomas Unterthiner, Jessica Yung, Andreas Steiner, Daniel Keysers, Jakob Uszkoreit, et al., “Mlp-mixer: An all-mlp architecture for vision,” *Advances in Neural Information Processing Systems*, vol. 34, pp. 24261–24272, 2021.

[52] Kaiming He, Xiangyu Zhang, Shaoqing Ren, and Jian Sun, “Deep residual learning for image recognition,” in *2016 IEEE Conference on Computer Vision and Pattern Recognition (CVPR)*, 2016, pp. 770–778.

[53] Olaf Ronneberger, Philipp Fischer, and Thomas Brox, “U-net: Convolutional networks for biomedical image segmentation,” in *International Conference on Medical image computing and computer-assisted intervention*. Springer, 2015, pp. 234–241.

[54] Alexey Dosovitskiy, Lucas Beyer, Alexander Kolesnikov, Dirk Weissenborn, Xiaohua Zhai, Thomas Unterthiner, Mostafa Dehghani, Matthias Minderer, Georg Heigold, Sylvain Gelly, et al., “An image is worth 16x16 words: Transformers for image recognition at scale,” in *International Conference on Learning Representations*, 2020.

- [55] Clark Glymour, Kun Zhang, and Peter Spirtes, “Review of causal discovery methods based on graphical models,” *Frontiers in genetics*, vol. 10, pp. 524, 2019.
- [56] Manabu Kuroki and Judea Pearl, “Measurement bias and effect restoration in causal inference,” *Biometrika*, vol. 101, no. 2, pp. 423–437, 2014.
- [57] Judea Pearl, *Probabilistic reasoning in intelligent systems: networks of plausible inference*, Morgan kaufmann, 1988.
- [58] Dan Geiger, Thomas Verma, and Judea Pearl, “d-separation: From theorems to algorithms,” in *Machine Intelligence and Pattern Recognition*, vol. 10, pp. 139–148. Elsevier, 1990.
- [59] Zejian Li, Yongchuan Tang, Wei Li, and Yongxing He, “Learning disentangled representation with pairwise independence,” in *Proceedings of the AAAI Conference on Artificial Intelligence*, 2019, vol. 33, pp. 4245–4252.
- [60] Karsten Roth, Mark Ibrahim, Zeynep Akata, Pascal Vincent, and Diane Bouchacourt, “Disentanglement of correlated factors via hausdorff factorized support,” *arXiv preprint arXiv:2210.07347*, 2022.
- [61] Muhammad Waleed Gondal, Manuel Wuthrich, Djordje Miladinovic, Francesco Locatello, Martin Breidt, Valentin Volchkov, Joel Akpo, Olivier Bachem, Bernhard Schölkopf, and Stefan Bauer, “On the transfer of inductive bias from simulation to the real world: a new disentanglement dataset,” *Advances in Neural Information Processing Systems*, vol. 32, 2019.
- [62] Cian Eastwood and Christopher KI Williams, “A framework for the quantitative evaluation of disentangled representations,” in *International Conference on Learning Representations*, 2018.

A Background

A.1 Directed acyclic graphs

In the context of causality, the data generation process of a measurement $\mathbf{x} \in \mathbb{R}^N$ is represented by a directed acyclic graph (DAG) [27]. The DAG provides the mathematical language for expressing domain knowledge through transparent and testable assumptions about the underlying causal relationships. In this framework, domain variables are represented as nodes, directed edges express causal relationships between variables and their functional relationships are described by distributions p defined over variables. DAG’s operate under the Markov compatibility property which states that the joint distribution p is compatible with a DAG G or that G represents p if it admits the product decomposition

$$p(x_1, \dots, x_n) = \prod_i p(x_i | pa_i). \quad (7)$$

Variables pa_i are the Markovian parents of x_i that belong to the minimal set of predecessors of x_i that renders x_i independent of all its other predecessors; in other words that, $p(x_i | pa_i) = p(x_i | x_1, \dots, x_{i-1})$ [49]. This Markov property restricts the unbounded number of plausible models that can fit the joint distribution to only those that are compatible with the specified decomposition. However, causal models are not only about this Markov restriction shared also by Bayesian networks [57], but more than that, they aim to move relationships between variables beyond mere correlation into causation. Causal inference analysis provides the axioms to establish causality by predicting the effects of interventions from the assumed DAG and ordinary distributions of observations. The effects of interventions written as $do(x = x)$ or more compactly as \hat{x} represent how external agents may affect the system by forcing certain variables to take on predefined values. These axioms branded under the *do*-calculus are presented in Section A.2.

A.2 *do*-calculus

d-Separation denoted by $X \perp\!\!\!\perp Y | \mathbf{Z}$ implies conditional independence of X and Y given a set of variables \mathbf{Z} in every distribution compatible with the DAG, while absence of *d-Separation* implies the converse; a dependence in almost all distributions compatible with the DAG [58]. Variables X and Y are *d-Separated* given Z if and only if Z blocks every path from node X to node Y [27]. The two conditions for blocking are:

- In the paths $i \rightarrow m \rightarrow j$ or $i \leftarrow m \rightarrow j$ the node m is in Z , or

- there is a collider $i \rightarrow m \leftarrow j$ where neither node m nor its descendant is in Z .

In terms of notation, in a DAG G , $G_{\overline{X}}$ and $G_{\underline{X}}$ denote, respectively, the graphs obtained by deleting the incoming and outgoing arrows at node X .

The rules of interventional *do*-calculus according to Pearl are given as [27, 49]:

Rule 1 (Insertion/deletion of observations):

$$p(y|\hat{x}, z, w) = p(y|\hat{x}, w) \quad \text{if } (Y \perp\!\!\!\perp Z)|X, W)_{G_{\overline{X}}}$$

Rule 2 (Action/observation exchange):

$$p(y|\hat{x}, \hat{z}, w) = p(y|\hat{x}, z, w) \quad \text{if } (Y \perp\!\!\!\perp Z)|X, W)_{G_{\overline{X}\underline{Z}}}$$

Rule 3 (Insertion/deletion of actions):

$$p(y|\hat{x}, \hat{z}, w) = p(y|\hat{x}, w) \quad \text{if } (Y \perp\!\!\!\perp Z)|X, W)_{G_{\overline{X}\overline{Z}}}$$

These graphical rules encompass the foundational principles of the *do*-calculus [27]. By analyzing the DAG and employing these rules, it becomes possible to characterize the effects of interventions $do(x)$ in terms of ordinary probability distributions of observations. This process, known as identification in the context of causal inference, serves as the primary analytical tool for elevating relationships between variables from mere correlation to causation.

A.3 Example

As an example, consider the learning problem $p(y|x)$ (e.g., label prediction y from observations x) where we observe three variables x, y, z from a joint distribution $p(x, y, z)$. In the absence of a data generation process model, this problem can be expressed as $p(y|z) = \sum_z p(x, y, z)/p(x)$. A DL model for solving this problem would learn a function that fits the joint distribution over the observed variables. However, there are numerous models that can fit this distribution, such as $p(x, y, z) = p(y|z)p(z|x)p(x)$, $p(x|z)p(z|y)p(y)$, $p(y|x, z)p(x)p(z)$, and many more combinations of variables. The issue arises because each of these decompositions represents a specific generative model, and without any restrictions, the DL model is free to choose any of them. This can be problematic as there exists many models that do not align to domain knowledge and this can invoke a variety of additional problems. For example, DL models that lack interpretability or that fail at transfer in the presence of data distribution shifts. Imposing a data generative model through DAG's thus constrains the DL model to align its behavior with the specified DAG.

In the specific case example shown in Fig.5a, the DL model fitting the joint distribution over the observations would align with the generative model represented by the decomposition $p(x, y, z) = p(y|x, z)p(x|z)p(z)$. However, a potential issue arises as z influences both the independent variable x and the dependent variable y , leading to spurious correlations between variables and introducing a potential source of bias for the learning problem $p(y|x)$. Lifting this model from correlation to

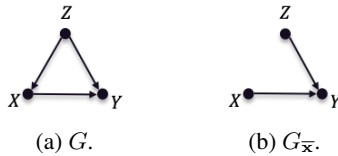


Figure 5: DAG example

causation through the application of *do*-calculus rules, tackles this issue by analyzing the system in terms of interventions. Utilizing *do*-calculus, we can reformulate the learning problem as $p(y|\hat{x})$, and

its identification can be expressed as:

$$p(y|\hat{x}) = \sum_z p(\hat{x}, y, z)/p(\hat{x}) \quad (8)$$

$$= \sum_z p(y|z, \hat{x})p(\hat{x}|z)p(z)/p(\hat{x}) \quad (9)$$

$$= \sum_z p(y|z, \hat{x})p(\hat{x})p(z)/p(\hat{x}) \quad (10)$$

$$= \sum_z p(y|z, x)p(z) = \mathbb{E}_z p(y|z, x) \quad (11)$$

where Eq.(10) follows since conditioning on parent variables has no effect on interventions. Eq.(11) follows by noting that x and y are d -separated under Fig.5b. As such, we can exchange the action $p(y|\hat{x}, z)$ for the observation $p(y|x, z)$ as described by Rule 2 of the *do*-calculus. A DL model that learns by fitting $p(y|\hat{x})$ from Eq.(11) instead of $p(y|x)$ aligns with the causal data generation process encoded by the DAG. This alignment, helps alleviate potential sources of bias that can be identified in the system, as made transparent through the DAG. In our proposed research, we are driven by the fundamental premise that causal models offer both superior disentanglement and representation of domain knowledge compared to mere correlations. To incorporate these causally derived constraints, we leverage derived distributions over interventions $p(y|\hat{x})$ and reformulate the learning problem accordingly.

B Identification of Causal Relationships

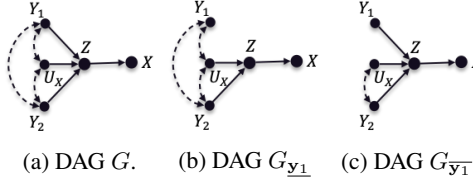


Figure 6: A DAG with colliders

Identification of the causal effects $p(\mathbf{z}|\hat{\mathbf{y}}_c)$ in Eq.(1) involves application of the rules of the *do*-calculus by leveraging the causal assumptions encoded in the DAG. This is used to convert probabilities of interventions to expressions involving only ordinary probabilities of observations. The DAG in Fig.6a is a representation of the data generative model of independent factors $p(\mathbf{y}) = \prod_{c=1}^n p(\mathbf{y}_c)$ assumed in [5, 15, 12, 17] and a simplification of Fig.1. In this case however, with only three factor variables $\mathbf{y}_1, \mathbf{y}_2, \mathbf{u}_x$. The DAG structure in Fig.6a contains a collider at \mathbf{z} . A collider is represented in a DAG by a node where two or more arrows or paths converge. When conditioning on or controlling for a collider, it can induce an association between its causes, even if they are not causally related. This phenomenon is known as collider bias or selection bias [28, 29, 26]. In this case, conditioning on the collider \mathbf{z} can introduce a spurious association between its causes $\mathbf{y}_1, \mathbf{y}_2, \mathbf{u}_x$. This needs to be accounted for, when training a DL model to learn from $p(\mathbf{x}, \mathbf{z}, \mathbf{y}, \mathbf{u}_x)$, otherwise it is prone to produce biased models. Again, we do this through derivations involving the effects of interventions $p(\mathbf{z}|\hat{\mathbf{y}}_1)$ in the system encoded by Fig.6a. Application of the law of total probability in Eq.(12) and the chain rule in Eq.(13) yields:

$$p(\mathbf{z}|\hat{\mathbf{y}}_1) = \sum_{\mathbf{y}_2, \mathbf{u}_x} p(\mathbf{z}, \hat{\mathbf{y}}_1, \hat{\mathbf{y}}_2, \mathbf{u}_x)/p(\hat{\mathbf{y}}_1) \quad (12)$$

$$= \sum_{\mathbf{y}_2, \mathbf{u}_x} p(\mathbf{z}|\hat{\mathbf{y}}_1, \mathbf{y}_2, \mathbf{u}_x)p(\hat{\mathbf{y}}_1|\mathbf{y}_2, \mathbf{u}_x)p(\mathbf{y}_2, \mathbf{u}_x)/p(\hat{\mathbf{y}}_1) \quad (13)$$

$$= \sum_{\mathbf{y}_2, \mathbf{u}_x} p(\mathbf{z}|\hat{\mathbf{y}}_1, \mathbf{y}_2, \mathbf{u}_x)p(\mathbf{y}_2, \mathbf{u}_x) \quad (14)$$

$$= \sum_{\mathbf{y}_2, \mathbf{u}_x} p(\mathbf{z}|\mathbf{y}, \mathbf{u}_x)p(\mathbf{y}_2, \mathbf{u}_x) = \mathbb{E}_{\mathbf{y}_2, \mathbf{u}_x} [p(\mathbf{z}|\mathbf{y}, \mathbf{u}_x)] \quad (15)$$

Eq.(14) follows by definition of the *do* operator implying no effect on an intervention conditioned on any variables (i.e., $p(\hat{\mathbf{y}}_1|\mathbf{y}_2) = p(\hat{\mathbf{y}}_1)$). Eq.(15) follows as Rule 2 for action/observation exchange is satisfied. In other words, given that $(\mathbf{Z} \perp\!\!\!\perp \mathbf{Y}_1) | (\mathbf{Y}_2, \mathbf{U}_x)_{G_{\mathbf{y}_1}}$ is d -separated in $G_{\mathbf{y}_1}$ in Fig.6b allows the exchange from $p(\mathbf{z}|\hat{\mathbf{y}}_1, \mathbf{y}_2, \mathbf{u}_x)$ to $p(\mathbf{z}|\mathbf{y}_1, \mathbf{y}_2, \mathbf{u}_x)$ and since $\mathbf{y} = [\mathbf{y}_1, \mathbf{y}_2]$ by our definition, completes the proof. Extensions to cases where $n > 2$ as in the generative model in Sec.2.1 follows trivially through the same derivation.

Abusing causal notation, we derive the identifiability conditions of the query $p(\mathbf{z}|\mathbf{x}, \hat{\mathbf{y}}_1)$ in Eq.(5) noting that all terms involved respect the causal direction.

$$p(\mathbf{z}|\mathbf{x}, \hat{\mathbf{y}}_1) = p(\mathbf{x}|\mathbf{z}, \hat{\mathbf{y}}_1)p(\mathbf{z}|\hat{\mathbf{y}}_1)p(\hat{\mathbf{y}}_1)/p(\mathbf{x}, \hat{\mathbf{y}}_1) \quad (16)$$

$$= p(\mathbf{x}|\mathbf{z}) \mathbb{E}_{\mathbf{y}_2, \mathbf{u}_x} [p(\mathbf{z}|\mathbf{y}, \mathbf{u}_x)] / p(\mathbf{x}, \mathbf{y}_1) \quad (17)$$

Eq.(16) follows by application of the chain rule of probability. Deletion of actions from $p(\mathbf{x}|\mathbf{z}, \hat{\mathbf{y}}_1)$ follows by applying Rule 3, satisfied when d -separation $(\mathbf{X} \perp\!\!\!\perp \mathbf{Y}_1) | (\mathbf{Z})_{G_{\hat{\mathbf{y}}_1}}$ is satisfied. By inspection of Fig.6c we see this is indeed the case. Also, the action $p(\hat{\mathbf{y}}_1)$ is by definition one and substituting the result of the conditional latent distribution $p(\mathbf{z}|\hat{\mathbf{y}}_1)$ in Eq.(15) completes writing an equivalent expression involving only ordinary probabilities of observations for the numerator. An expression for the denominator $p(\mathbf{x}, \hat{\mathbf{y}}_1)$ follows by adding \mathbf{z} through the law of total probability and using the chain rule as $\sum_z p(\mathbf{x}, \hat{\mathbf{y}}_1|\mathbf{z})p(\mathbf{z})$. The action/observation exchange $\sum_z p(\mathbf{x}, \mathbf{y}_1|\mathbf{z})p(\mathbf{z})$ then follows by checking if $(\mathbf{X} \perp\!\!\!\perp \mathbf{Y}_1) | (\mathbf{Z})_{G_{\mathbf{y}_1}}$ is satisfied; which is indeed the case by inspection of Fig.6b, completing the proof.

When at least one of the generating factors, such as \mathbf{u}_x (e.g., sensor noise), remains unmeasured, it will leave several paths (e.g., $\mathbf{y}_1 \leftrightarrow \mathbf{u}_x, \mathbf{y}_1 \leftrightarrow \mathbf{u}_x \leftrightarrow \mathbf{y}_2$) in the collider unblocked. This means, the causal effect of \mathbf{y}_1 on \mathbf{z} cannot be identified uniquely, but only a relaxed relationship where $p(\mathbf{z}|\hat{\mathbf{y}}_1)$ may carry information correlations with both \mathbf{u}_x and \mathbf{y}_2 . The strength of such correlations depends in this case on the energies of \mathbf{u}_x relative to \mathbf{z} . But, overall the strength of these correlations has a direct impact on the severity of bias in DL models. This problem can be aggravated exponentially when the number of unmeasured generating factors increases. One of the main arguments in this research is that collider bias is prevalent in the majority of DL models designed to disentangle generative factors. These models often fall short in recognizing and effectively addressing this issue. We propose leveraging the power of causal models, specifically DAGs, to effectively incorporate a transparent and explicit model of the generative process. This integration aims to identify and mitigate the influence of colliders on disentanglement tasks. By leveraging DAGs, we can enhance the understanding and management of collider effects, improving the overall performance of disentanglement DL models.

C ELBO

Training a DL model by fitting the distribution over the observables only, yields an unbounded number of plausible DL models. We could only hope that the fitting function returns a model that aligns with a data generative model that has some meaning to the domain knowledge. However, this is rarely the case in practice, even in the presence of just a few generating variables. Through ReI, we align the VAE framework, with the causal DAG of Fig.6a through a reformulation of the ELBO that accounts for the presence of a collider. The reformulation describes the learning problem in terms not of the ordinary posterior $q(\mathbf{z}|\mathbf{x}, \mathbf{y})$ but rather in terms of an interventional posterior $q(\mathbf{z}|\mathbf{x}, \hat{\mathbf{y}})$. Derivation of this reformulated ELBO in Eq.(6) follows the same steps as in [5] starting with the Kullback-Leibler (KL) divergence.

$$D_{KL}(q(\mathbf{z}|\mathbf{x}, \hat{\mathbf{y}}_c) || p(\mathbf{z}|\mathbf{x}, \hat{\mathbf{y}}_c)) = - \sum q(\mathbf{z}|\mathbf{x}, \mathbf{y}_c) \log p(\mathbf{z}|\mathbf{x}, \hat{\mathbf{y}}_c) / q(\mathbf{z}|\mathbf{x}, \mathbf{y}_c) \quad (18)$$

$$= - \mathbb{E}_{q(\mathbf{z}|\mathbf{x}, \mathbf{y}_c)} \{ \log p(\mathbf{x}|\mathbf{z}) \} - \sum q(\mathbf{z}|\mathbf{x}, \mathbf{y}_c) \log \mathbb{E}_{p(\mathbf{w}_c)} [p(\mathbf{z}|\mathbf{y})] / q(\mathbf{z}|\mathbf{x}, \mathbf{y}_c) + \log p(\mathbf{x}, \mathbf{y}_c). \quad (19)$$

Eq.(18) follows by definition of the KL divergence, while Eq.(19) substitutes the result from the identification adjustments for the causal query $p(\mathbf{z}|\mathbf{x}, \hat{\mathbf{y}}_c)$ in Eq.(17). Based on Eq(19), the ELBO can be written as in Eq.(20), completing its derivation. Note that in Eq.(20) we have omitted the

presence of a factor \mathbf{u}_x and focused only on the observed factors \mathbf{y}_c .

$$\begin{aligned} & \log p(\mathbf{x}^{(i)}, \mathbf{y}_c^{(i)}) \geq \mathcal{L}(\theta, \phi; \mathbf{x}^{(i)}, \mathbf{y}_c^{(i)}) \\ &= \mathbb{E}_{q(\mathbf{z}|\mathbf{x}^{(i)}, \mathbf{y}_c^{(i)})} \left\{ \log p(\mathbf{x}^{(i)}|\mathbf{z}) \right\} - D_{KL} \left(q(\mathbf{z}|\mathbf{x}^{(i)}, \mathbf{y}_c^{(i)}) \parallel \mathbb{E}_{\mathbf{w}_c} [p(\mathbf{z}|\mathbf{y})] \right). \end{aligned} \quad (20)$$

D Benchmark experiments

We include additional experiments that show and compare the performance of DL models with ReI against state of the art methods on the task of disentanglement. In this task, the compared works [5, 15, 12, 17, 24] assume the joint distribution of the generating variables can be decomposed by independence of factors: i.e., $p(\mathbf{y}) = \prod_{c=1}^n p(\mathbf{y}_c)$. This data generative model works under the idealized conditions that datasets contain no correlations between factors. However, in practice, real datasets rarely preserve this condition and more than often generating factors present strong correlations in training data [59, 45, 25, 60]. Extensions to disentanglement methods that address this non-ideal setting appeared in [25, 60] where pairs of factors are synthetically correlated. ReI in this case integrates instead a DAG of the generative model containing a collider as in Fig.6a and Fig.1 and reformulates the VAE objective to align with the DAG that mitigates the influence of this collider on the disentanglement task. We argue, both uncorrelated and correlated generative factors can be better expressed and modeled through a DAG structured as a collider as in Fig.1. We perform experiments that compare performance on this task on both the uncorrelated and the correlated training data settings against state of the art methods. The datasets used are the standard ML benchmarks used for learning disentangled representations: Shapes3D [17], dSprites [15] and MPI3D [61]. These datasets have been used for this specific task in the works of [15, 12, 17, 24, 25].

D.1 Quantitative Evaluations

The metric of disentanglement performance used here is DCI (Disentanglement, Completeness, Informativeness) scores [62]. DCI has been established as the most widely accepted metrics of disentanglement performance [13, 24, 25, 60]. DCI evaluations are performed in synthetic datasets generated by either independent or by correlated factors. For the later, we use the extensions in [60] to correlate one, two and three generative factor pairs (where applicable) and one to all factors (1-to-all). Correlations in the generated data is produced by the method described in [25, 60] with σ quantifying the amount of correlation between factors. The smaller the σ , the stronger the correlation is, and viceversa. All pair-wise correlations where generated with $\sigma = 0.1$, while a $\sigma = 0.2$ was used to generate the factor correlated with all others (i.e., 1-to-all). This is consistant with the experiments conducted in [25, 60]. We report the average metric computed over 10 seeds and present the results in Tables 2, 3 and 4 for all three datasets.

Table 2: DCI-Disentanglement Performance Comparison on **dSprites** [15]

Method	Uncorr.	Pairs: 1	Pairs: 2	1-to-All
β -VAE	32.3	9.4	7.8	11.3
Factor-VAE	25.2	13.1	14.1	14.4
β -TCVAE	31.3	23.9	11.3	20.3
Annealed-VAE	39.2	14.8	8.7	14.2
β -VAE + HFS	43.2	19.2	12.5	14.5
VAE + ReI	87.5	88.2	88.1	89.4

In tables 2, 3 and 4 we see that the DCI performance degrades throughout all datasets as the number of correlated pairs increase for most of the methods compared. These do not seem to be well equipped to handle an increasing number of correlated generating factors. The observed degradation can be explained by the behavior of a collider implicit in the independent generative model $p(\mathbf{y}) = \prod_{c=1}^n p(\mathbf{y}_c)$ and described in Appendix.B. In the presence of a collider, generative factors become correlated when conditioning on the common effect, unless a supervisory measurement is available per factor to block its effects. The severity of this spurious correlations depends on the number of factors that remain unidentified. The fact that the compared methods do not address

Table 3: DCI-Disentanglement Performance Comparison on **Shapes3D** [17]

Method	Uncorr.	Pairs: 1	Pairs: 2	Pairs: 3	1-to-All
β -VAE	70.3	71.2	51.6	36.5	36.3
Factor-VAE	62.3	70.8	58.7	46.1	31.9
β -TCVAE	77.4	70.2	63.4	38.8	51.9
Annealed-VAE	62.1	55.7	30.8	36.2	23.1
β -VAE + HFS	86.3	79.6	66.3	49.7	63.4
VAE + ReI	95.9	96.6	96.3	96.1	95.8

Table 4: DCI-Disentanglement Performance Comparison on **MPI3D** [61]

Method	Uncorr.	Pairs: 1	Pairs: 2	Pairs: 3	1-to-All
β -VAE	25.9	18.3	23.7	11.3	11.2
Factor-VAE	26.6	22.8	28.2	11.0	13.8
β -TCVAE	27.3	20.9	22.8	11.1	514.5
Annealed-VAE	11.4	12.3	11.9	10.7	13.1
β -VAE + HFS	32.9	29.2	27.3	13.8	15.7
VAE + ReI	73.5	72.6	74.3	71.9	73.5

this collider behavior explicitly, explains the lower performance as the number of correlated pairs increases in the benchmark datasets. By explicitly addressing this type of collider bias by leveraging the power of causal models, the performance of ReI remains more or less invariant to the number of correlation pairs in as long as the effects of the generating factors remains identifiable. This is one of the main benefits of ReI, which of course comes at the cost of requiring some form of measurement or mechanism to identify the effects of each generating factor. In the case of the benchmark datasets evaluated here, there are labels for each of these factors which are exploited by ReI.

In contrast to dSprites and Shapes3D datasets, the MPI3D dataset comes from real images captured from a moving robotic arm. The relatively lower performance of all methods on this dataset can be attributed to the fact that it represents real-world scenarios with several unmeasured factors of variation. The images in MPI3D are obtained from three different cameras each affected by sensor noise, blur, illumination changes from view, etc. Failing to account for variations from these variables ultimately leads we believe to a degradation in overall performance. The presence of unaccounted variables, along with the open paths connecting them to the observed generative factors in a DAG that exhibits a collider structure (as shown in Figures 1 and Fig. 6a), can explain the potential origins of spurious correlations that induce the biased results, thus resulting in the degraded performance.

D.2 DL model settings

The VAE architectures used throughout the benchmarking experiments follows the implementations of [24, 60]. The encoder consists of 2x [Conv(32,4,4) + ReLU], 2x [Conv(64,4,4) + ReLU], MLP(256), MLP(2x10). The Decoder uses: MLP(256), 2 x [upConv(64,4,4) + ReLU], 2 x [upConv(32,4,4) + ReLU], [upConv(3,4,4) + ReLU]. Inputs are images with 3 channels grouped into batches of 64 images. Training is performed using the Adam optimizer with a learning rate of 10e-4 for 300,000 training steps. In the case of Factor-VAE, the architecture includes six layers of [MLP(1000), leakyReLU] followed by an MLP(2).

D.3 DCI

The DCI disentanglement metric [62] is a measure of how each variable (or dimension) captures at most one generative factor. It can be computed for each variable or dimension i as $D_i = (1 - H_K(P_i))$. Here, $H_K(P_i)$ is entropy given as $H_K(P_i) = -\sum_{k=0}^{K-1} P_{ik} \log_K P_{ik}$ and $P_{ij} = R_{ij} / \sum_{k=0}^{K-1} R_{ik}$ is the probability of a learned latent variable being important for predicting a known generating factor. This later (i.e., R_{ij}) can be computed from the classification prediction error.

D.4 Concluding Remarks

We conclude this subsection by highlighting an additional significant drawback of the state of the art methods for disentanglement in comparison to ours: they do not produce representations that align with domain knowledge. This limitation carries significant drawbacks in high-risk applications, including domains such as healthcare, financial risk assessment, and energy reliability. It also extends to other fields where the need for highly interpretable models is paramount, such as scientific research. In these contexts, the ability to understand and interpret the underlying factors driving model predictions is crucial for making informed decisions and ensuring the reliability and safety of the outcomes. Addressing this limitation becomes particularly vital in such applications. These domains often demand cautious adoption of DL models due to the potential consequences of biased predictions. As a result, the integration of DL approaches has progressed at a slower pace in these areas, emphasizing the need for thorough consideration of the limitations and potential risks associated with these models.